HHS Public Access

Author manuscript

ACS Biomater Sci Eng. Author manuscript; available in PMC 2020 April 02.

Published in final edited form as:

ACS Biomater Sci Eng. 2019 September 9; 5(9): 4551–4563. doi:10.1021/acsbiomaterials.9b00505.

A Visible Light-Cross-Linkable, Fibrin–Gelatin-Based Bioprinted Construct with Human Cardiomyocytes and Fibroblasts

Shweta Anil Kumar[†,&], **Matthew Alonzo**[†,&], **Shane C. Allen**[§], **Laila Abelseth**[‖,⊥], **Vikram Thakur**[▽], **Jun Akimoto**[○], **Yoshihiro Ito**[○,◆], **Stephanie M. Willerth**[‖,⊥,#,¶], **Laura Suggs**[§], **Munmun Chattopadhyay**[▽], **Binata Joddar**[*,†,‡,○]

[†]Inspired Materials & Stem-Cell Based Tissue Engineering Laboratory (IMSTEL), Department of Metallurgical, Materials and Biomedical Engineering, M201 Metallurgy Building, United States

[‡]Border Biomedical Research Center, University of Texas at El Paso, 500 West University Avenue, El Paso, Texas 79968, United States

[§]Department of Biomedical Engineering, The University of Texas at Austin, 110 Inner Campus Drive, Austin, Texas 78712, United States

[‖]Department of Mechanical Engineering, University of Victoria, Engineering Office Wing, Room 548, 3800 Finnerty Road, Victoria, British Columbia V8P 5C2, Canada

[⊥]Biomedical Engineering Program, University of Victoria, Engineering Office Wing, Room 548, 3800 Finnerty Road, Victoria, British Columbia V8P 5C2, Canada

[#]Division of Medical Sciences, University of Victoria, Engineering Office Wing, Room 548, 3800 Finnerty Road, Victoria, British Columbia V8P 5C2, Canada

[▽]Department of Molecular and Translational Medicine, Center of Emphasis in Diabetes and Metabolism, Texas Tech University Health Sciences Center, 5001 El Paso Drive, El Paso, Texas 79905, United States

[○]Nano Medical Engineering Laboratory, RIKEN Custer for Pioneering Research, 2-1 Hirosawa, Wako, Saitama 351-0198, Japan

[◆]Emergent Bioengineering Materials Research Team, RIKEN Center for Emergent Matter Science, 2-1 Hirosawa, Wako, Saitama 351-0198, Japan

[*]**Corresponding Author:** bjoddar@utep.edu. Tel.: +1-(915)-747-8456. Fax: +1-(915)-747-8036.

[&]S.A.K. and M.A. share equal contribution as first authors in this manuscript. S.A.K. and M.A. performed the experiments repeatedly and collected and analyzed the data. L.A. and S.W. prepared and provided the fibrinogen solutions in varying concentrations and provided technical inputs. S.A.K., M.A., and B.J. wrote the manuscript and prepared all the figures. S.C.A. and L.S. performed rheology and analyzed the resultant data. V.T. and M.C. facilitated the CM and CF cultures, cell coupling experiments, and their microscopic imaging along with images and writing of relevant sections in the manuscript. J.A. and Y.I. provided the furfuryl–gelatin and performed cytotoxicity assay for Rose Bengal. All authors reviewed the manuscript and provided their consent for publication. The manuscript was written through individual contributions of all authors. All authors have given approval to the final version of the manuscript.

Supporting Information

The Supporting Information is available free of charge on the ACS Publications website at DOI: 10.1021/acsbiomaterials.9b00505. Description for fibrinogen preparation, preparation of gel-fu, cytotoxicity assessment for Rose Bengal, evaluation of the cell orientation in bioprinted constructs, and preparation of sections for immunostaining (PDF)

The authors declare no competing financial interest.

¶International Collaboration on Repair Discoveries, University of British Columbia, 818 West 10th Avenue, Vancouver, British Columbia V5Z 1M9, Canada

Abstract

In this study, fibrin was added to a photo-polymerizable gelatin-based bioink mixture to fabricate cardiac cell-laden constructs seeded with human induced pluripotent stem cell-derived cardiomyocytes (iPS-CM) or CM cell lines with cardiac fibroblasts (CF). The extensive use of platelet-rich fibrin, its capacity to offer patient specificity, and the similarity in composition to surgical glue prompted us to include fibrin in the existing bioink composition. The cell-laden bioprinted constructs were cross-linked to retain a herringbone pattern via a two-step procedure including the visible light cross-linking of furfuryl–gelatin followed by the chemical cross-linking of fibrinogen via thrombin and calcium chloride. The printed constructs revealed an extremely porous, networked structure that afforded long-term in vitro stability. Cardiomyocytes printed within the sheet structure showed excellent viability, proliferation, and expression of the troponin I cardiac marker. We extended the utility of this fibrin–gelatin bioink toward coculturing and coupling of CM and cardiac fibroblasts (CF), the interaction of which is extremely important for maintenance of normal physiology of the cardiac wall in vivo. This enhanced “cardiac construct” can be used for drug cytotoxicity screening or unraveling triggers for heart diseases in vitro.

GRAPHICAL ABSTRACT

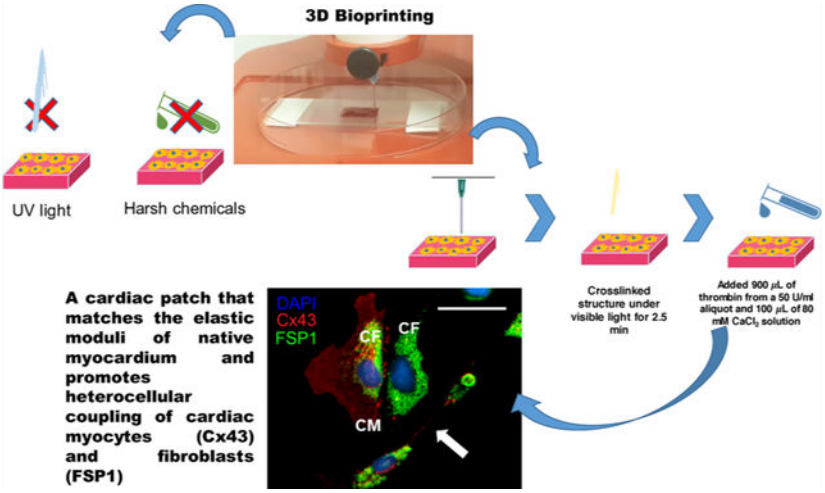

Keywords

fibrinogen; thrombin; furfuryl–gelatin; biofabrication; 3D bioprinting; cardiac tissue

INTRODUCTION

Myocardial infarction, or the irreversible death of cardiomyocytes (CM), is one of the leading causes of morbidity and mortality worldwide.[1] This condition, caused by the deposition of plaque to the arterial walls that supply the heart with blood, results in prolonged ischemia to the myocardium.[2] Death to millions of CM, and hence, the necrosis

of cardiac muscle tissue, is a direct consequence of the poor blood flow needed to sustain cellular vitality. Furthermore, the minimal intrinsic ability of the heart to regenerate itself following an injury makes the condition further life-threatening as CM are terminally differentiated cells.[3] Following damage to the myocardium, a dense collagenous scar tissue is formed by fibroblasts,[4] limiting the contractile efficiency of the heart and can further cause heart failure in the long term.[5]

Current strategies for the treatment of end-stage heart failure include organ transplant surgeries,[6] use of ventricular assist devices,[7] and cellular cardiomyoplasty,[8] all of which aim to restore the functional ability of the heart. However, tissue engineering of CM-laden 3D printed constructs that can be potentially implanted in vivo comes across as a better alternative as they can be created from cells in a scaffold material that is intended to mimic the native extracellular matrix (ECM).[9] These cell-containing scaffolds are more readily vascularized by the host's circulatory system and are also cost-effective,[10] can be readily engineered, and most importantly, will reduce the probability of an immune response as the cells may be obtained autologously from patients.[11]

Among a wide range of polymeric materials investigated for their application in the fabrication of such tissue-engineered, ECM-mimicking "cardiac constructs", gelatin continues to be one of the most popular materials because of its biocompatibility and low immunogenicity. We had previously developed a novel furfuryl–gelatin (gel-fu)-based bioink that was cross-linkable by visible light for the fabrication of mono- and bilayered bioprinted scaffolds that successfully cultured mouse mesenchymal stem cells in the former and cocultured STO fibroblasts and C2C12 myoblasts in the latter.[12] The cells were observed to exhibit good viability and heterocellular coupling even after several days of culture. However, the rheology study performed on the aforementioned scaffolds revealed an elastic modulus of 1.7 kPa, which is significantly lower than that of the native myocardium that has been determined to be ~9 kPa.[13] This created an immediate need for a biomaterial to be used in tandem with gel-fu to develop a scaffold with a modulus closely mimicking the mechanical properties of the native heart tissue. The extensive and widespread usage of fibrin as a surgical sealant[14] and as tissue engineering scaffolds[15] made it the most natural choice to be incorporated as an additive for the development of a cardiac construct. The present study incorporates fibrin into the previously mentioned gel-fu-based bioink to test its feasibility as a scaffold for the culture of CM as it is known to promote vascularization,[16] envisioning a future in vivo application of this laboratory-engineered cardiac construct.

The fibrin–gelatin-based bioink was used to print square-shaped constructs laden with human CM. The preparation of the fibrin–gelatin bioink and the fabrication of the square-shaped 3D constructs have been described under the Materials section. The printed constructs were subjected to a dual-step cross-linking process, first by subjecting them to visible light to facilitate the cross-linking of the gel-fu, followed by the addition of a thrombin–$CaCl_2$ solution to the samples to induce the cross-linking of fibrinogen to fibrin. The acellular scaffold was characterized using material analysis techniques, as done previously.[12] This fibrin–gelatin-based bioink was used to bioprint human induced pluripotent stem cell (iPSC)-derived CM or human CM cell lines to show their cytocompatibility. Next, we investigated the ability of this substrate to promote

heterocellular coupling between bioprinted human cardiac fibroblasts (CF) and CM to validate the applicability of this scaffold toward mimicking cardiac tissue, often classified by the presence and crosstalk of these two essential cell types.

MATERIALS AND METHODS

Materials.

Furfuryl–gelatin[17,18] and fibrinogen[19] solutions ranging from 10 to 60 mg/mL were prepared as described in previous studies. Rose Bengal (RB) was procured from Thermo Fisher Scientific (Waltham, MA, USA). Furfuryl–gelatin or gel-fu was prepared by homogeneous addition of furfuryl glycidyl ether to a porcine gelatin solution, as detailed in the Supporting Information.

Biofabrication.

For biofabrication, an Allevi 2 (formerly the BioBot 1, Allevi, Philadelphia, PA, USA) was used. To make 1 mL of the bioink, 990 μL of fibrinogen solution (60 mg/mL) was mixed with 155 mg of gel-fu at 25 °C. The mixture was then heated at 37 °C for 1 h with stirring to facilitate the formation of a homogeneous and viscous mixture. RB (10 μL) was subsequently added as a photosensitizer and mixed homogeneously with the existing bioink mixture.[17,20]

Optimization of the fibrinogen solution concentration and the gel-fu amounts for making the bioink is described in Table 1 below.

The concentration of fibrinogen solution used in the present study (60 mg/mL) was based on a previous study conducted by Cui and Boland.[21] This study had shown that the best polymerization result obtained via bioprinting was observed with 60 mg/mL fibrinogen, 50 units/mL thrombin, and 80 mM $CaCl_2$. Cells were added to this bioink mixture as described later in the Biocompatibility section. These results served as the basis for our present study[21] as lower concentrations of fibrinogen solution (50 mg/mL) did not yield bioinks that were printable.

The bioink mixture was loaded into a 10 mL plastic syringe (BD, Franklin Lakes, NJ, USA) fitted with a stainless steel blunt-tip dispensing needle (Huaha, Amazon, USA) and extruded using a low extrusion pressure (18–25.5 kPa). Patterns printed using this bioink were designed using SolidWorks (Concord, MA, USA) and saved as .stl files. The structures were square-shaped having dimensions of 1 cm × 1 cm and a thickness of 500 μm and were printed on 100 mm × 15 mm Petri dishes (ThermoFisher). The .stl file used for printing was uploaded to the Repetier Host program available via the Allevi server, which converted it into a G-code. The G-code file was then uploaded and used to print structures, which were subjected to a dual-step cross-linking process, first by exposing them to 400 nm wavelength visible light for an optimized duration of 2.5 min at 100% intensity (IntelliRay 600, Uvitron International, West Springfield, MA, USA) based on our previous study.[12] Second, the chemical cross-linking of fibrinogen into fibrin was induced by exposing the printed constructs to a 1 mL solution composed of 900 μL of 80 mM $CaCl_2$ and 100 μL of thrombin in PBS at a concentration of 50 units/mL for ~20 min.

Material Characterization of the Printed Acellular Structures.

Scanning Electron Microscopy.—Images of the dried gels were obtained following previously published procedures.[22] The sample used for the imaging of the cross sections was synthesized, dried overnight in a chemical fume hood, and visualized using a table-top scanning electron microscope (SEM; TM-1000, Hitachi, Japan) at a voltage of 15 kV at 10,000× magnification. The images acquired were analyzed using ImageJ to determine the average pore size of the samples assessed.

Swelling Assay.—The hydration behavior of the hydrogel was studied by performing a swelling assay. Initially, the gels were allowed to swell to equilibrium for 5 days in Dulbecco modified Eagle's medium (DMEM, pH = 7, 25 °C), following published protocols.[22] Three identical printed structures were cross-linked and stored at −80 °C overnight before being freeze-dried using a VirTis BenchTop Pro Freeze Dryer with Omnitronics (SP Scientific, Warminster, PA, USA). These freeze-dried samples were weighed (W_0) and immersed in DMEM, and their swollen weights (W_t) were monitored periodically after every 24 h for 5 days. The swelling ratio was calculated using eq 1, where D_s is the degree of swelling.[22]

$$D_s = \frac{W_t - W_0}{W_0} \quad (1)$$

Rheology.—To perform the rheometric analysis, gels were made and cut out using biopsy punches (~1 mm deep, 8 mm diameter) for testing. The gels were allowed to swell in 1× PBS for about an hour before testing. An Anton-Paar MCR101 rheometer (Anton-Paar, Graz, Austria) with an 8 mm parallel plate geometry was employed to perform oscillatory shear stress rheometry (1% strain, 0.5–50 Hz). The strain and frequency range analyzed by frequency sweep were within the linear viscoelastic range of the gels tested. Complex shear modulus was calculated as a function of the storage and loss moduli, and the complex viscosity was measured at 1.99 Hz for all samples, as done before.[23] Furthermore, the viscoelastic behavior of the gels was evaluated from 0.05 to 500 Hz, but the elastic modulus was determined through a shorter sweep from 0.5 to 50 Hz.

Fourier Transform Infrared Spectroscopy Analysis.—Fourier transform infrared spectroscopy (FTIR) was used to reveal information about the dual cross-linked structure after exposure to visible light irradiation and the thrombin–$CaCl_2$ solution, in comparison with the control sample that is composed of the gel-fu and fibrinogen solution mixed together but not exposed to visible light nor cross-linked with thrombin–$CaCl_2$. A PerkinElmer Spectrum 100 Universal ATR Sampling Accessory within the range of 650–3650 cm^{-1} in the transmittance mode was used to acquire the attenuated total reflectance (ATR)-FTIR spectra of the representative samples, as was done before.[24] Spectral analysis software GRAMS/32 (Galactic Industries Corp., Salem, NH, USA) was used to perform spectral manipulations. An s-polarized beam at an angle of incidence of 40° and a mercury cadmium telluride (MCT/A) detector were used to record the external reflection FTIR on a Specac grazing angle accessory. The background consisted of a Piranha-treated silicon wafer.

Cell Culture, Characterization, and Viability in Bioprinted Constructs.

Human induced pluripotent stem cell (iPSC)-derived cardiomyocytes (CM) were obtained from Axol Bioscience (U.K.), and human CM AC16 cell lines (ATCC) were cultured and stabilized prior to experiments. For the human iPSC-derived CM, cells were bioprinted and cultured for a day to test the compatibility of this technique and the bioink materials toward primary cell culture, viability, and retention. About 2×10^5 cells/mL were added and printed within casted 3D patterns and cultured in an incubator (37 °C, 5% CO_2). Controls seeded in 2D wells (24 wells) received 5×10^4 cells/mL. This difference in cell seeding density was because cells in 3D structures had to spread over a larger volume compared to their 2D controls. After 24 and 72 h, respectively, the cultures were analyzed using a Live/Dead assay (Thermo Fisher Scientific, Waltham, USA) with Calcein AM (green) that stained the live cells and ethidium homodimer (red) that stained the dead cells. After 24 h of culture, the cell-laden constructs were processed for immunochemistry and stained with antibodies against troponin T (Anti-Cardiac Troponin T antibody [1C11], Abcam, MA, USA) to validate their functionality and cardiac-specific characteristics in bioprinted constructs (as detailed in the Supporting Information).

A similar procedure was employed for the human CM AC16 cells that were seeded and then subjected to the Live/Dead assay. All Live/ Dead stained cells were then imaged using a confocal fluorescence microscope (Olympus IX81 inverted fluorescence motorized microscope, Japan) to confirm the retention of viable cells within the bioprinted structures.

To validate the cardiac smooth muscle specificity of the human CM AC16 lines, the cells were immunostained with Myocardin (Myocd, Novus Biologicals, 1:200) antibody to confirm their phenotype as well as their sarcomeric organization. Additionally, we confirmed the integrity of the CM by co-immunostaining with a characteristic cardiac biomarker, troponin T (TrpT, Cell Signaling, 1:300).

Biocompatibility.

To check the biocompatibility of the fibrin–gelatin-based bioink, human CM that were encapsulated in this mixture for printing were probed for their expression of troponin I, a cardiac marker after sustained in vitro culture. At the end of culture, the cells in bioprinted constructs were fixed with 4% paraformalde-hyde (Sigma) for 15 min (25 °C). Post fixation, these cell-laden constructs were permeabilized with 0.2% Triton X-100/PBS for 1 h.

After blocking with 1% normal goat serum (NGS/PBS, Sigma) overnight at 4 °C, the samples were incubated with a rabbit polyclonal antibody to troponin I (at a dilution of 1:1000, 24 h at 4 °C) followed by an anti-rabbit secondary antibody at a concentration of 1:4000 (2 h at 25 °C) (Thermo Fisher Scientific). The samples were then washed thrice with 1× PBS, mounted using Fluoromount-G with DAPI (ThermoFisher Scientific), and imaged using a confocal fluorescence microscope (Olympus IX81 inverted fluorescence motorized microscope, Japan). Acquired images were processed using ImageJ to assess the preferential cell orientation along the printing direction in comparison with nonbioprinted samples (as detailed in the Supporting Information).

To confirm viable cell encapsulation within the bioprinted constructs, prior to addition in the bioink mixture, the CM were labeled with PKH26 red fluorescent membrane staining dye (Sigma), as done before,[12] and imaged after 24 h of culture without fixing the cells in the gel samples using a confocal fluorescence microscope (Zeiss).

To assess the cytotoxicity of the Rose Bengal in the bioink, cell viability was determined and tracked over a period of 5 days, as explained in the Supporting Information.

Coupling of Human Cardiomyocytes and Fibroblasts in Vitro.

Human CM (AC16) and adult human fibroblasts (Cell Applications Inc.) were cultured and passaged using complete growth media for the respective cell types, following vendors' suggested protocols. For the coupling experiment, cells from early passages (3–4) were used. The sample groups included both 3D printed gels and 2D tissue culture wells. For both wells and gels, cells were coupled in a ratio of CM/CF (1:1) based on the published literature.[25] Prior to addition in the bioink mixture, the CM were labeled with PKH26 red fluorescent membrane staining dye, and the CF were labeled with PKH67 green dye (Sigma), as done before.[12] Cells were mixed in the desired ratios, while the cell seeding density was maintained at 1×10^4 cells/mL for the 2D wells and 2×10^5 cells/mL for the 3D gels. Since the 3D gels provided more surface area for cell attachment and growth compared to the 2D wells, the cell density for these respective substrates were altered accordingly. For the 3D gels, cells were mixed in the bioink, and the gels were printed and cross-linked as described earlier. After 24 h of culture, cells were counterstained with DAPI and imaged using a confocal microscope. Controls included CM prestained with PKH26 and CF, prestained with PKH67, and seeded in wells. All cells were incubated with DAPI prior to imaging. Representative fluorescent images were acquired using a confocal microscope (Nikon). In addition, viable and nonfixed cells were also used to confirm heterocellular coupling between CM and CF. The CM were prestained with PKH26, and the CF were prestained with PKH67, as explained above. For biofabrication of a grid structure (5 mm × 5 mm), two separate bioink mixtures with 1×10^7 cells/mL were made using CM and CF and printed into a lattice pattern using a BioBot 1 (Allevi, USA). Controls included cells randomly mixed in gels and cross-linked. Since CF are known to electronically communicate between groups of CM via junction connections established through Cx43,[26] to confirm their heterocellular coupling, they were cultured in a 1:1 ratio for a total of 6 h with and without the addition of Gap26, a Cx43 inhibitor.[27] Specifically, to confirm the effects of the Cx43 blocker, Gap26, a dose optimization study was done utilizing 15, 30, and 50 μM of this inhibitor compound on the heterocellular coupled cultures.[28] Cells (CM–CF) cultured without the addition of Gap26 served as controls in this experiment. In addition, CM only, cultured with and without the addition of Gap26, were stained for Cx43 and served as additional controls. The cultured constructs were processed to isolate individual sections that are 8–10 μm thick (as detailed in the Supporting Information). These sections were immunostained as done previously[29] and probed with FSP-1 (for CF, 1:400, Sigma), troponin I (for CM, 1:400, Thermo Fisher), and Cx43 (1:500, Cell Signaling) antibodies. This was followed by addition and incubation with either goat anti-rabbit IgG secondary antibody/Alexa Fluor 594 or goat anti-mouse IgG secondary antibody/Alexa Fluor 488 conjugate, both of which are applied at a dilution of 1:1000. Cocultures of CM and CF were

immunostained with troponin I and FSP-1 to identify individual cell types, either CM or CF as controls. The samples were then washed thrice with 1× PBS, mounted using Fluoromount-G with DAPI (Thermo Fisher Scientific), and imaged using a confocal fluorescence microscope (Nikon). Acquired images were processed and analyzed using NIS elements (Nikon) to obtain the signal intensity for the expression of Cx43 across various samples cultured with and without the addition of Gap26.

In addition, to compare the quantified expression of Cx43 in CM in bioprinted versus nonbioprinted controls, samples were also stained for Cx43 and imaged as described above.

Statistical Analysis.

All samples were present in groups of three, unless otherwise specified. Data are represented as the mean ± standard deviation. Comparison of the means of two independent samples was performed by *t*-test (IBM SPSS) to determine if the averages of any two of the sample datasets compared showed significant difference in their values. $P < 0.05$ was considered statistically significant. The datasets generated during and/or analyzed during the current study are available from the corresponding author upon reasonable request.

RESULTS

The square structure was constructed using CAD software and converted into an .stl file, which we adopted to print the fibrin–gelatin-based cardiac constructs (Figure 1A). The .stl file shows the herringbone pattern, so named due to its resemblance to the cardiac muscle tissue.[30] The gross morphological en face SEM image of a 3D printed square pattern fabricated using the fibrin–gelatin bioink was captured as shown in Figure 1B. The architecture of the design was maintained through a dual cross-linking procedure, as described earlier. An actual pattern deposited by the 3D bioprinting process is also shown (Figure 1C).

Specifically, the bioprinted cell-laden construct was irradiated with 400 nm visible light for 2.5 min at 100% intensity (IntelliRay 600, Uvitron International, West Springfield, MA, USA) based on parameters optimized during our previous study.[12] Right after, thrombin–calcium chloride ($CaCl_2$) solution was cast on the structure for 20 min to chemically cross-link fibrinogen into fibrin. A representative cross-sectional image of a printed square pattern generated by SEM as shown in Figure 2A indicated a porous geometry with interconnected pores that appeared to be well distributed and equal-sized. A representative cross-sectional image of a gel-fu-based rectangular printed pattern generated by SEM is shown in Figure 2B for comparison. The average pore diameter (endto-end length) was determined to be 9.54 ± 0.98 μm for the fibrin–gelatin-based constructs in comparison with 15.62 ± 3.05 μm for the gel-fu patterns. These values were significantly different, with $P = 0.0032$. Enhancing the cross-linking density of gelatin using fibrin would decrease its porosity compared to gelatin, [31] which is implied by our results. However, the average pore size of these scaffolds is in the permissible range for cardiovascular tissue engineering and angiogenesis.[32,33] A comparative analysis of the average pore sizes of the fibrin–gelatin-based square pattern and the gelatin-based rectangular sheet that was fabricated in our previous study[12] was performed (Figure 2C).

These results led us to conclude that the pore size of the fibrin–gelatin-based structure was slightly reduced in comparison to the previous study,[12] which may be attributed to the herringbone pattern, the addition of fibrin, and the dual cross-linking chemistry adopted in this study.

The swelling behavior of the printed structures when the samples were submerged in cell culture media is depicted in Figure 3. Results showed that the maximum swelling of the tested samples occurred after 96 h (4 days) after which the scaffolds had reached an equilibrium swelling degree. This time point was achieved much later compared to our previous study wherein samples reached equilibrium swelling ratios after only 24 h (1 day) in culture ($p = 0.02$).[12] This proves that the dual cross-linking scheme led to the generation of constructs with enhanced structural fidelity compared to our previously published study.[12]

Rheometric analysis performed on discs acquired from the fibrin–gelatin printed structures yielded results, as shown in Figure 4. Amplitude and frequency sweeps were performed to determine if the strain and frequency range were within the linear viscoelastic range of the gels. As shown in Figure 4A, the elastic modulus was found to be 9.76 kPa, which is comparable to that of the native myocardium.[13] The complex viscosity calculated at an angular frequency of 1.99 Hz was 1.63 Pa·s. The average storage and loss moduli for the tested samples (samples #1 and #2) were determined (Figure 4B). The higher storage modulus in both cases indicates that the elastic behavior of the gel predominates over its viscous nature, characteristic of a stably cross-linked hydrogel.[23]

Fourier-transform infrared (FTIR) spectra of the fibrin–gelatin printed constructs were analyzed to validate the formation of the cross-linked composite, as presented in Figure S1A. Peaks for fibrin appeared at ~1636, 1533, and 1238 cm^{-1}, characterizing the protein's amide I, amide II, and amide III vibrations, respectively.[34–36] In addition, the CH_2 deformation in the protein's structure is seen at ~1451 cm^{-1} with amino acid side-chain vibrations appearing at ~1400 cm^{-1}, similar to the published literature.[36] The f-gelatin vibrational mode corresponding to the C=O stretching is found near 1636 cm^{-1} and N–H and C–N stretching modes at 1530 cm^{-1}. The deformation of the =C—H bond in the furan ring is shown at ~920 cm^{-1}, similar to the published literature.[37] A broad band corresponding to the N–H vibrational mode is observed at 3282 cm^{-1}.

The spectra from two controls, namely, spectra (a) showing signatures for the non-cross-linked gelatin–fibrinogen composite and spectrum (b) showing only photopolymerization of the f-gelatin component are also illustrated in Figure S1B. Although no major differences can be seen between the raw composite mixture and the photopolymerized mixture, the cross-linking of fibrinogen into fibrin is confirmed by the appearance of the vibrational mode of C–N stretching at ~1150–1000 cm^{-1}, similar to the published literature.[38]

A Live/Dead assay was performed by incorporating both human iPSC-derived CM and human CM separately during the 3D printing of the fibrin–gelatin-based constructs (Figure 5A and Figure S2) to confirm if human induced pluripotent stem cell (iPSC)-derived CM (Axol Bioscience, UK) and CM cell lines (adult human ventricular CM, AC16, ATCC) could withstand the extrusion printing and cross-linking phenomenon. Human iPSC-derived

CM having a short shelf life made it necessary to employ the human CM cell lines additionally to confirm the results exhibited by the primary cultures used. These human CM cell lines exhibited a sarcomeric structure when probed using appropriate biomarkers, confirming their functional and morphological resemblance with human cardiomyocytes (Figure S3).

The Live/Dead assay performed on human CM cell lines printed within the fibrin–gelatin-based constructs and imaged after a duration of 5 days of culture is depicted in Figure 5A along with 2D culture controls (Figure S4A). The characteristic images of human iPSC-derived CM, which were bioprinted within fibrin–gelatin patterns and imaged using the Live/Dead assay, are included in Figure S2A,B. Troponin T staining (red) validated the presence of cardiac myocytes within the bioprinted constructs (Figure S2C). Further, the human CM cell lines that were bioprinted within the fibrin–gelatin-based constructs and stained with troponin I[39] and DAPI were imaged after 5 days (Figure 5B). Troponin I is a marker used to positively stain and characterize CM expression in cultures.[39] It was observed that there was an increased number of cells, confirming the biocompatibility of the fibrin–gelatin-based gel with the human CM encapsulated within printed constructs (Figure 5B). The characteristic 2D controls for troponin I-stained images of human CM cell lines, which were cultured in tissue culture wells and imaged after 24 h, respectively, are shown in Figure S4B. Figure 5C depicts viable human CM imaged within fibrin–gelatin printed patterns after 24 h of culture. Cells were seen to align along the herringbone pattern and form networks, as seen in the representative image in Figure 5C. On the contrary, nonprinted controls for cells in gels shown in Figure S4C do not exhibit any pattern in cell alignment. Moreover, the thickness of the gel cannot be controlled when casted manually, which hinders with the visual detection of the encapsulated cells (Figure S4C). Thus, the herringbone pattern was specifically advantageous as cells were guided by the herringbone design to form networks that may eventually lead to cardiomyogenesis.

In all the confocal microscopy images that were obtained post Live/Dead assay (Figure 5A), the percentage of dead cells (8 ± 4%) was found to be negligible as compared to the live cells (92 ± 3%) (Figure 5D). These values were significantly different with $p = 0.0012$. These trends did not alter after 72 h when the percentage of dead cells was estimated to be 10 ± 5% compared to the live cells at 98 ± 4%. Overall, both human iPSC-derived CM and CM cell lines could withstand the extrusion printing and dual cross-linking phenomena, as depicted by our results. The minimal extent of cell death observed in our study implied that the bioink material and the printing parameters used did not pose any harmful effect to the encapsulated cells and can support the cell viability without disrupting the constructs, on the basis of past research.[40–42]

These results were confirmed from cell proliferation estimation (human CM lines) where the characteristic cell count was found to be 2.82×10^5 and 9.6×10^5 cells/mL after 24 and 72 h, respectively, in the 3D printed constructs, with respect to the 2D culture systems (controls) where the cell density increased from 1.24×10^5 to 4.34×10^5 cells/mL for the same duration (Figure 5E). The cells seeded in the fibrin–gelatin scaffolds were found to proliferate equally as the cells cultured in the 2D culture systems, implying that the fibrin–

gelatin scaffolds were favorable for the cells and directed cellular growth and proliferation (Figure 5E).

The presence of in vitro heterocellular coupling between the two cell types, namely, electrically excitable cardiomyocytes (CM) and the nonexcitable cardiac fibroblasts (CF), is a relatively well-known and established phenomenon.[43–45] It is understood that CF act as long-distance conductors and can electronically bridge gaps between groups of CM via gap junctions and connections established by Cx43, the loss or reduced expression of which is linked to fibrosis due to enhanced fibroblast activity. This kind of excitation–contraction coupling is responsible for contractile activity in the cardiac muscle.[46] We were interested in simulating the dynamics of this in vivo heterocellular coupling phenomenon between CF and CM using this fibrin–gelatin-based bioink in vitro. We applied this fibrin–gelatin-based bioink to perform a coupling experiment using human CM and CF when both cell types were present in equal proportions. The coupling experiment performed using human CM and CF seeded in tissue culture wells and in the bioprinted constructs yielded images, as shown in Figures 6 and 7, following 24 h of incubation. These representative images of coupling are comparable to those found in the existing literature.[26,47]

Images shown in Figure 6A,D are derived from coupling experiments of CM/CF (1:1) imaged in 2D wells and in 3D bioprinted gels, respectively. Nonprinted controls that included cells mixed in gels are shown in Figure S5A. We noted the characteristic elongated and rod-shaped morphologies of the CM (Figure 6A). Furthermore, viable cell behavior and heterocellular coupling of CM and CF were confirmed by results depicted in Figure 7 as nonfixed cells were used for imaging in this case. In fact, cells (CM–CF) present in nonbioprinted samples embedded in bulk did not show any preferential pattern, showing a random cellular orientation (Figure S5B–E), as also supported by a published work.[48] On the contrary, 3D bioprinted cell clusters revealed a higher long-range cellular organization (Figure 6D and Figure S5F–I). Figure 6E shows a comparison of plotted average intensity values representing cell density and cell orientation within the zone marked by the white dotted lines (in Figure 6D) in a characteristic bioprinted sample (black) versus a nonbioprinted sample (gray). The average intensity values for the bioprinted samples (black) exhibited more frequent peaks within the range depicted, indicating a higher frequency of cells present in the preferred orientation compared to samples that were nonbioprinted (gray) (Figure 6E).

Since the CM were coupled with CF, resulting in the establishment of junctions possibly leading to secretion of ECM, this may have caused the change in the morphology to a more typical rod shape for the CM (Figures 6A and 7), as characterized in vivo.[49] These results very strongly imply that CM and CF can be coupled in vitro, enabling their interactions to be probed to study the resultant downstream effects, which may play a key role in development and disease conditions. Very interestingly, we also observed that a greater number of cells per unit area exhibited coupling in the 3D gels compared to the 2D wells as the gels allowed more range for the cells to communicate and interact, mimicking a physiologically relevant environment (Figures 6D and 7). This observation lays the foundation and provides justification for a 3D bioprinted model for making organoids that are made up of two to three different cell types to mimic complex in vivo tissue physiology.

Heterocellular coupling between CM and nonexcitable CF has been known to occur via specific adhesion junctions such as connexin-43 (Cx43).[46] To confirm this pathway in our study, the CM and CF cultured in a 1:1 ratio were stained with troponin I, a specific CM marker,[50] and fibroblast-specific protein 1 (FSP-1), a specific fibroblast marker, which showed uniform coupling of these two cell types. As adhesion junctions between CM and CF are a critical factor in cell–cell interactions, the cultures were stained for Cx43 to confirm the heterocellular coupling in these cells (Figure 8A–F). To confirm their heterocellular coupling in the absence of Gap26, cocultures of CM and CF were immunostained with troponin I and FSP-1, which enabled identification and confirmation of phenotypes for these cells (Figure S6A,B). In addition, the expression of Cx43 from CM only with and without the addition of Gap26 is shown in Figure S7.

The effects of a dose-dependent inhibition of the heterocellular coupling between CM and CF by applying various concentrations of Gap26, a Cx43 inhibitor,[27] were observed (Figure 8B,C,E,F). Briefly, among a dose range of 15, 30, and 50 μM, the dose of 15 μM Gap26 showed significant reduction in the expression of Cx43 and inhibition of cell–cell coupling, which was linearly dependent on the dose of Gap26 (Figure 8B,E,G). The results from 15 and 30 μM Gap26 are depicted in Figure 8C,F,G), while 50 μM data is not shown. Controls that did not receive any Gap26 (no treatment) show significant expression of Cx43 (Figure 8G, $P < 0.001$) and cell–cell coupling (Figure 8A,D and Figure S6A,B). Specifically, in these no-treatment images, we found evidence of long-distance intercellular connectivity between CM and CF (depicted with an arrow in Figure 8A), which is believed to be mediated by membrane nanotubes.[51] Furthermore, we found evidence of CF coupling atop CM and adjoined with a neighboring CF (Figure 8A), which pointed toward a “double-sided coupling”, as described in the literature.[46] This double-sided coupling refers to cardiac fibroblast connections that interlink cardiac myocytes, which are not directly coupled electrically.[46]

Connexin-43 (Cx43; red) expression was also compared and quantified across AC16 cardiomyocytes, either 3D bioprinted or in controls prepared by randomly mixing cells in gels and cross-linking them. We found that the 3D bioprinted samples expressed a distinct pattern of cell alignment and connectivity that enhanced the expression of Cx43 in these samples (Figure S8). It is well known that the cell alignment and function of cardiomyocytes are extremely important for the proper function of cardiac tissue and maintenance of normal cardiac physiology. Therefore, our results strongly imply that adopting 3D printing clearly poses irreplaceable benefits on mimicking the native tissues structure and function, which is clearly lacking in controls (Figure S8).

Finally, we report on the effects of RB on cell-encapsulated hydrogels in this study (Figure S9). Although RB was gradually released from the f-gelatin-based hydrogels, the cells exhibited a growth behavior similar to controls, and no significant toxicity was observed. Almost all the cells exhibited green fluorescence derived from calcein AM when stained after 24 h of culture, indicating cell viability in the presence of RB. These observations confirmed that the RB released from the f-gelatin hydrogels imposed no significant influence on the cell viability.

DISCUSSION

Bioprinting is a versatile approach that can be applied toward fabricating structurally complex scaffolds,[52] targeted drug delivery,[52] disease modeling,[53] and drug screening.[54] We have employed 3D bioprinting to encapsulate physiologically high cell densities to mimic in vivo cell densities within rectangular cell-laden structures,[12] while others have focused on employing 3D printing to mimic complex geometries.[55] Furthermore, we were also successful in printing bilayered sheets with dissimilar cell types separately encapsulated in the top and bottom layers, which added uniqueness to our approach and enabled us to mimic multilayered tissues present in vivo.

Prior to 3D bioprinting being widely adopted by many, cardiac patches were fabricated using other methods such as using PDMS molds used by Zhang et al. to culture fibrin-based cardiac patches laden with human embryonic stem cell-derived CM.[56] Although tissue engineering of a cardiac patch was attempted previously via 3D bioprinting by others,[57,58] we were the first to utilize a naturally derived, visible light-curable mixture of furfuryl–gelatin and hyaluronic acid (HA)[12] for ioprinting this cell-laden construct. Other groups have engineered composite hydrogels using two naturally derived biopolymers, gelatin and tropoelastin via visible light-induced cross-linking, for wound healing applications.[59] Visible light-induced cross-linking does not induce DNA alterations, causing immunosuppression in vivo, or have any detrimental effects on the cell viability, as was observed in previous studies that employed techniques such as UV cross-linking[60–62] and chemical cross-linking,[63,64] making it a safer alternative. However, in our previous study, the optimized bioink mixture consisting of gel-fu and hyaluronic acid (HA) revealed an elastic modulus of only 1.7 kPa for the cross-linked gels. Although this allowed us to encapsulate multiple cell types within different layers, the mechanical stiffness of the substrate is not well matched to be used as a cardiac tissue-mimicking scaffold.[65]

The bioink that was used in the current study was formulated by incorporating a fibrinogen solution in addition to the gel-fu, HA, and Rose Bengal (RB) mixture that was used in our past work.[12] However, HA was excluded from this study as it was not chemically cross-linked within the bioprinted constructs.[12] The urge to apply a fibrinogen-based bioink was derived from the extensive use of platelet-rich fibrin (PRF).[66] Platelet-rich plasma (PRP) is a concentrate of platelet-rich plasma protein with an increased concentration of autologous platelets that form a suspension in plasma after centrifugation.[67] Platelet-rich fibrin (PRF) is a second-generation PRP where autologous platelets and leucocytes are present within a complex matrix of fibrin with wide-ranging applications in tissue engineering, owing to its ability to accelerate soft and hard tissue healing.[66] Although both PRP and PRF are patient-specific as they are both derived from the patients' own blood, PRF is considered to be superior due to its slow polymerization during centrifugation, fibrin-based structure, ease of formulation, and minimal cost.[66] Recently, it has been extensively used in biomedical applications such as in wound healing,[68] in dentistry,[69] and as a surgical sealant.[70] Its widespread use and its ability to offer patient specificity prompted us to include fibrinogen in our bioink as a matrix biomaterial. A prior study has established the efficacy of employing fibrin glue as an injectable scaffold that could preserve the infarct wall thickness and the cardiac function following myocardial infarction in rats and may be useful as a

biomaterial scaffold in myocardial cell transplantation.[71] Some other studies have also validated the utility of fibrin-based scaffolds for delivering CM to the myocardium.[72–76] Thus, we anticipate that this fibrin–gelatin-based cardiac construct can be made by using patient-derived PRF in the future, thereby reducing the possibility of immunorejection and favoring rapid in vivo implantation. In addition, the gel-fu is visible light-cross-linkable that facilitates prompt application[17,20,77] and has been shown to be well tolerated in vivo.[20] Biofabrication of this composite cell-laden construct via bioprinting will enable the addition of desired cell types, densities, and multilayered configurations of multiple cell types, which are not feasible by other methods. However, fibrin by itself does not possess the necessary mechanical stiffness for tissue engineering applications, thereby necessitating the need to incorporate another component while developing the bioink. So, imparting structural integrity and better mechanical properties through a dual-step cross-linking method, including a first visible light-induced cross-linking (gel-fu and RB) followed by chemical cross-linking (fibrinogen with thrombin℃$CaCl_2$), is a novel approach that has been never adopted before. This dual cross-linking procedure yielded an elastic modulus of 9.6 kPa, which closely resembles that of the native myocardium.[13] Prior studies with fibrin have incorporated chemical cross-linkers such as genipin[15,78] and glutaraldehyde,[79] which have been reported to be potentially toxic to cells.[63] On the contrary, the fibrin–gelatin scaffolds utilized in this study favored cell growth and proliferation with a negligible dead cell count, indicating that the dual-step cross-linking imposed no toxicity on the cell population encapsulated within the constructs. In the future, we will seek to assess the efficacy of these cardiac constructs made from CM to engraft and limit cardiac left ventricular remodeling acutely after infarction in a rat model also.[72]

Cardiomyogenesis refers to the renewal and growth of cardiomyocytes lost in injury or disease. A major limitation in treating cardiac injury is the failure of current therapies to induce myocardium regeneration and cardiomyogenesis.[72–76,80] One possible avenue for resolving this situation is to engineer cardiac tissues by 3D bioprinting. This technique can lead to engineered cardiac tissue that can structurally mimic the anatomy and details of in vivo tissues.[72–76,80] In this study, the herringbone pattern induced cell alignment and growth and may promote cardiomyogenesis in future in vivo studies. The importance of designing scaffolds for mimicking cardiac tissue with appropriate mechanical properties has also been emphasized by other studies as these scaffolds have shown to improve cell alignment and supported the cardiac-specific functionality of the cells embedded.[81] The dual cross-linking procedure included the photo-cross-linking performed first followed by chemical cross-linking of fibrinogen with thrombin and $CaCl_2$, which could have possibly imparted additional stiffness to the bioprinted constructs, in comparison to our previous work.[12] This was done to reduce the exposure time of the cells to the unreacted RB, which could have possibly produced a toxic effect on them.[82] Therefore, this led to the formation of a stable, porous, and well-networked structure, allowing the cells to communicate by crosstalk and grow well within these scaffolds. Further, this added stability also lead to the fibrin–gelatin scaffolds exhibiting significantly lower swelling ratios at later time points compared to the gelfu-based scaffolds used in our previous study.[12]

Troponin I was used to stain positively for the CM as it has been widely used as a cardiac marker.[83] However, it is also known that troponin I and troponin T are both upregulated

during ischemic heart disease, which also categorizes them as markers of stress.[83] According to our data, the expression for troponin I was stronger after 5 days of culture compared to after 24 h (not shown), which implied enhanced cell growth and expansion in the culture. However, the cells definitely did not appear stressed or unviable, in which case, they would appear to be fragmented and undergoing apoptosis. In future, we will attempt to characterize the CM cultures based on their expression of other cardiac markers such as α-actinin.[84]

Myocardin (Myocd) is a potent transcriptional coactivator expressed exclusively in cardiac myocytes during postnatal development.[85] Myocd is required for maintenance of the cardiomyocyte structure and sarcomeric organization, and its loss in cardiac myocytes leads to programmed cell death.[85] The ablation of the Myocd gene is known to be accompanied by dissolution of sarcomeric organization and apoptosis of cardiac myocytes.[85] Therefore, Myocd is often utilized as a popular biomarker for depicting the saromeric structure of cardiac myocytes, as done in this study.

CONCLUSIONS

In summary, we formulated a fibrin–gelatin-based bioink useful toward targeted bioprinting of CM-laden constructs with mechanical properties identical to that of the native myocardial tissue. We may encapsulate human iPSC-derived CM and human CM and CF in these bioprinted scaffolds. The printed constructs retained good viability after sustained culture, indicating that the fibrin–gelatin-based bioink is a promising material for the fabrication of constructs that could be potentially used to repair the diseased myocardium and serve as a high-fidelity model for the study of cardiac diseases and for drug screening. Furthermore, we were successful in coupling both CM and CF in these visible light-cross-linkable and bioprinted cell–gel constructs. Although others have used a combination of different cell types such as endothelial cells (EC) and smooth muscle cells (SMC) for seeding in a cardiac construct,[86] we were the first to couple CM and CF, the two most relevant cell types for studying cellular physiology, interplay, and mechanisms for disease modulation in the cardiac wall.[87] In addition, immunochemistry data obtained in this study very clearly demonstrated this heterocellular coupling between CM and CF via Cx43 adhesion junctions, which is critical for cell–cell interactions. This was confirmed by the data from the Gap26 dose-dependent study, which showed linear reduction in cell–cell coupling with increasing doses of Gap26.

Supplementary Material

Refer to Web version on PubMed Central for supplementary material.

ACKNOWLEDGMENTS

We acknowledge Brian Roman, Nishat Tasnim, and Tahmina Akhter for technical assistance. M.A. acknowledges the Eloise E. and Patrick B. Wieland fellowship at UTEP and the Gates Millennium Scholarship Program. We acknowledge the technical assistance received from Armando Varela for kindly assisting us with the confocal microscopy and Michael Lyubchenko for his help with the SEM. The authors also acknowledge the help from Moinak Joddar, a senior at Radford School, El Paso, for image analysis using ImageJ for the development of Figure 6, E and Figure S5B-I.

Funding

The Willerth laboratory would like to acknowledge funding from the Stem Cell Network, the Canada Research Chairs program, the NSERC Discovery Grant program, MITACS, and the British Columbia Innovation Council. The Joddar laboratory (IMSTEL) acknowledges NIH BUILD Pilot 8UL1GM118970-02, NIH 1SC2HL134642-01, and the NSFPREM (DMR 1827745).

ABBREVIATIONS

CM	cardiac myocytes/cardiomyocytes
CF	cardiac fibroblasts
iPSC	induced pluripotent stem cells
ECM	extracellular matrix
RB	Rose Bengal
gel-fu	furfuryl–gelatin

REFERENCES

(1). Asaria P; Elliott P; Douglass M; Obermeyer Z; Soljak M; Majeed A; Ezzati M Acute myocardial infarction hospital admissions and deaths in England: a national follow-back and follow-forward record-linkage study. Lancet Public Health 2017, 2, e191–e201. [PubMed: 29253451]

(2). Stanford W; Thompson BH; Weiss RM Coronary artery calcification: clinical significance and current methods of detection. AJR, Am. J. Roentgenol 1993, 161, 1139–1146. [PubMed: 8249716]

(3). Ahuja P; Sdek P; MacLellan WR Cardiac myocyte cell cycle control in development, disease, and regeneration. Physiol. Rev 2007, 87, 521–544. [PubMed: 17429040]

(4). Sun Y; Weber KT Infarct scar: a dynamic tissue. Cardiovasc. Res 2000, 46, 250–256. [PubMed: 10773228]

(5). Thygesen K; Uretsky BF Acute ischaemia as a trigger of sudden cardiac death. Eur. Heart J. Suppl 2004, 6, D88–D90.

(6). Barnard CN The operation: a human cardiac transplant: an interim report of a successful operation performed at Groote Schuur Hospital, Cape Town. S. Afr. Med. J 2017, 107, 1271–1274.

(7). Rose EA; Gelijns AC; Moskowitz AJ; Heitjan DF; Stevenson LW; Dembitsky W; Long JW; Ascheim DD; Tierney AR; Levitan RG Long-term use of a left ventricular assist device for end-stage heart failure. N. Engl. J. Med 2001, 345, 1435–1443. [PubMed: 11794191]

(8). Chiu RCJ; Zibaitis A; Kao RL Cellular cardiomyoplasty: myocardial regeneration with satellite cell implantation. Ann. Thorac. Surg 1995, 60, 12–18. [PubMed: 7598572]

(9). Zhang J Engineered Tissue Patch for Cardiac Cell Therapy. Curr. Treat. Opt. Cardiovasc. Med 2015, 17, 399–399.

(10). Chia HN; Wu BM Recent advances in 3D printing of biomaterials. J. Biol. Eng 2015, 9, 4. [PubMed: 25866560]

(11). Vats A; Tolley NS; Bishop AE; Polak JM Embryonic stem cells and tissue engineering: delivering stem cells to the clinic. J. R. Soc. Med 2005, 98, 346–350. [PubMed: 16055897]

(12). AnilKumar S; Allen SC; Tasnim N; Akter T; Park S; Kumar A; Chattopadhyay M; Ito Y; Suggs LJ; Joddar B The applicability of furfuryl-gelatin as a novel bioink for tissue engineering applications. J. Biomed. Mater. Res., Part B 2019, DOI: 10.1002/jbm.b.34123.

(13). Boothe SD; Myers JD; Pok S; Sun J; Xi Y; Nieto RM; Cheng J; Jacot JG The Effect of Substrate Stiffness on Cardiomyocyte Action Potentials. Cell Biochem. Biophys 2016, 74, 527–535. [PubMed: 27722948]

(14). Jackson MR Fibrin sealants in surgical practice: an overview. Am. J. Surg 2001, 182, S1–S7.

(15). Ahmed TA; Dare EV; Hincke M Fibrin: a versatile scaffold for tissue engineering applications. Tissue Eng., Part B 2008, 14, 199–215.

(16). West JL; Moon JJ Vascularization of engineered tissues: approaches to promote angiogenesis in biomaterials. Curr. Top. Med. Chem 2008, 8, 300–310. [PubMed: 18393893]

(17). Park S-H; Seo S-Y; Kang J-H; Ito Y; Son T-I Preparation of photocured azidophenyl-fish gelatin and its capturing of human epidermal growth factor on titanium plate. J. Appl. Polym. Sci 2013, 127, 154–160.

(18). Park S.-h.; Seo S.-y.; Na H.-n.; Kim K.-i.; Lee J.-w.; Woo H.-d.; Lee J.-h.; Seok H.-k.; Lee J.-g.; Chung S.-i.; Chung K; Han D; Ito Y; Jang E.-c.; Son T.-i. Preparation of a visible light-reactive low molecular-O-carboxymethyl chitosan (LM-O-CMCS) derivative and applicability as an anti-adhesion agent. Macromol. Res 2011, 19, 921.

(19). Kolehmainen K; Willerth SM Preparation of 3D fibrin scaffolds for stem cell culture applications. J. Visualized Exp 2012, No. e3641.

(20). Mazaki T; Shiozaki Y; Yamane K; Yoshida A; Nakamura M; Yoshida Y; Zhou D; Kitajima T; Tanaka M; Ito Y; Ozaki T; Matsukawa A A novel, visible light-induced, rapidly cross-linkable gelatin scaffold for osteochondral tissue engineering. Sci. Rep 2014, 4, 4457. [PubMed: 24662725]

(21). Cui X; Boland T Human microvasculature fabrication using thermal inkjet printing technology. Biomaterials 2009, 30, 6221–6227. [PubMed: 19695697]

(22). Joddar B; Garcia E; Casas A; Stewart CM Development of functionalized multi-walled carbon-nanotube-based alginate hydrogels for enabling biomimetic technologies. Sci. Rep 2016, 6, 32456. [PubMed: 27578567]

(23). Stowers RS; Allen SC; Suggs LJ Dynamic phototuning of 3D hydrogel stiffness. Proc. Natl. Acad. Sci. U. S. A 2015, 112, 1953–1958. [PubMed: 25646417]

(24). Tasnim N; Kumar A; Joddar B Attenuation of the in vitro neurotoxicity of 316L SS by graphene oxide surface coating. Mater. Sci. Eng., C 2017, 73, 788–797.

(25). Zhou P; Pu WT Recounting cardiac cellular composition. Am. Heart Assoc 2016, 368.

(26). Kohl P; Camelliti P; Burton FL; Smith GL Electrical coupling of fibroblasts and myocytes: relevance for cardiac propagation. J. Electrocardiol 2005, 38, 45–50. [PubMed: 16226073]

(27). Hawat G; Benderdour M; Rousseau G; Baroudi G Connexin 43 mimetic peptide Gap26 confers protection to intact heart against myocardial ischemia injury. Pflügers Archiv-Eur. J. Physiol 2010, 460, 583–592. [PubMed: 20514543]

(28). Braet K; Vandamme W; Martin PEM; Evans WH; Leybaert L Photoliberating inositol-1, 4, 5-trisphosphate triggers ATP release that is blocked by the connexin mimetic peptide gap 26. Cell Calcium 2003, 33, 37–48. [PubMed: 12526886]

(29). Tasnim N; Thakur V; Chattopadhyay M; Joddar B The efficacy of Graphene-foams for culturing mesenchymal stem cells and Their differentiation into dopaminergic neurons. Stem Cells Int. 2018, 3410168. [PubMed: 29971110]

(30). Hughes SE The pathology of hypertrophic cardiomyopathy. Histopathology 2004, 44, 412–427. [PubMed: 15139989]

(31). Chimene D; Lennox KK; Kaunas RR; Gaharwar AK Advanced bioinks for 3D printing: A materials science perspective. Ann. Biomed. Eng 2016, 44, 2090–2102. [PubMed: 27184494]

(32). Loh QL; Choong C Three-dimensional scaffolds for tissue engineering applications: role of porosity and pore size. Tissue Eng., Part B 2013, 19, 485–502.

(33). Lu Q; Ganesan K; Simionescu DT; Vyavahare NR Novel porous aortic elastin and collagen scaffolds for tissue engineering. Biomaterials 2004, 25, 5227–5237. [PubMed: 15110474]

(34). Deepthi S; Jayakumar R Alginate nanobeads interspersed fibrin network as in situ forming hydrogel for soft tissue engineering. Bioact. Mater 2018, 3, 194–200. [PubMed: 29744457]

(35). Perumcherry SR; Chennazhi KP; Nair SV; Menon D; Afeesh R A Novel Method for the Fabrication of Fibrin-Based Electrospun Nanofibrous Scaffold for Tissue-Engineering Applications. Tissue Eng., Part C 2011, 17, 1121–1130.

(36). Tunc S; Maitz MF; Steiner G; Vázquez L; Pham MT; Salzer R In situ conformational analysis of fibrinogen adsorbed on Si surfaces. Colloids Surf., B 2005, 42, 219–225.

(37). García-Astrain C; Gandini A; Peña C; Algar I; Eceiza A; Corcuera M; Gabilondo N Diels–Alder "click" chemistry for the cross-linking of furfuryl-gelatin-polyetheramine hydrogels. RSC Adv. 2014, 4, 35578–35587.

(38). Stamatin L; Cristescu R; Socol G; Moldovan A; Mihaiescu D; Stamatin I; Mihailescu IN; Chrisey DB Laser deposition of fibrinogen blood proteins thin films by matrix assisted pulsed laser evaporation. Appl. Surf. Sci 2005, 248, 422–427.

(39). Bersell K; Savla J; Mollova M; Walsh S; DasLala T; Park S-Y; Silberstein L; dosRemedios C; Graham D; Colan S; Kuhn B Cardiomyocyte Proliferation Contributes to Heart Growth in young Humans. Circulation 2013, A15232.

(40). Wu Z; Su X; Xu Y; Kong B; Sun W; Mi S Bioprinting three-dimensional cell-laden tissue constructs with controllable degradation. Sci. Rep 2016, 6, 24474. [PubMed: 27091175]

(41). Faulkner-Jones A; Fyfe C; Cornelissen D-J; Gardner J; King J; Courtney A; Shu W Bioprinting of human pluripotent stem cells and their directed differentiation into hepatocyte-like cells for the generation of mini-livers in 3D. Biofabrication 2015, 7, No. 044102. [PubMed: 26486521]

(42). Rosenzweig DH; Carelli E; Steffen T; Jarzem P; Haglund L 3D-printed ABS and PLA scaffolds for cartilage and nucleus pulposus tissue regeneration. Int. J. Mol. Sci 2015, 16, 15118–15135. [PubMed: 26151846]

(43). Mark GE; Strasser FF Pacemaker activity and mitosis in cultures of newborn rat heart ventricle cells. Exp. Cell Res 1966, 44, 217–233. [PubMed: 5964748]

(44). Goshima K; Tonomura Y Synchronized beating of embryonic mouse myocardial cells mediated by FL cells in monolayer culture. Exp. Cell Res 1969, 56, 387–392. [PubMed: 5387911]

(45). Hyde A; Blondel B; Matter A; Cheneval JP; Filloux B; Girardier L Homo-and heterocellular junctions in cell cultures: an electrophysiological and morphological study. In Progress in brain research; Elsevier: 1969; Vol. 31, pp 283–311, DOI: 10.1016/S0079-6123(08)63247-1.

(46). Kohl P; Gourdie RG Fibroblast–myocyte electrotonic coupling: does it occur in native cardiac tissue? J. Mol. Cell. Cardiol 2014, 70, 37–46. [PubMed: 24412581]

(47). Gaudesius G; Miragoli M; Thomas SP; Rohr S Coupling of cardiac electrical activity over extended distances by fibroblasts of cardiac origin. Circ. Res 2003, 93, 421–428. [PubMed: 12893743]

(48). Maiullari F; Costantini M; Milan M; Pace V; Chirivì M; Maiullari S; Rainer A; Baci D; Marei HE-S; Seliktar D; Gargioli C; Bearzi C; Rizzi R A multi-cellular 3D bioprinting approach for vascularized heart tissue engineering based on HUVECs and iPSC-derived cardiomyocytes. Sci. Rep 2018, 8, 13532. [PubMed: 30201959]

(49). Bird SD; Doevendans PA; Van Rooijen MA; Brutel De La Riviere, A.; Hassink, R. J.; Passier, R.; Mummery, C. L. The human adult cardiomyocyte phenotype. Cardiovasc. Res 2003, 58, 423–434. [PubMed: 12757876]

(50). McLaurin MD; Apple FS; Voss EM; Herzog CA; Sharkey SW Cardiac troponin I, cardiac troponin T, and creatine kinase MB in dialysis patients without ischemic heart disease: evidence of cardiac troponin T expression in skeletal muscle. Clin. Chem 1997, 43, 976–982. [PubMed: 9191549]

(51). He K; Shi X; Zhang X; Dang S; Ma X; Liu F; Xu M; Lv Z; Han D; Fang X; Zhang Y Long-distance intercellular connectivity between cardiomyocytes and cardiofibroblasts mediated by membrane nanotubes. Cardiovasc. Res 2011, 92, 39–47. [PubMed: 21719573]

(52). Klein F; Richter B; Striebel T; Franz CM; von Freymann G; Wegener M; Bastmeyer M Two-component polymer scaffolds for controlled three-dimensional cell culture. Adv. Mater 2011, 23, 1341–1345. [PubMed: 21400593]

(53). Zhao Y; Yao R; Ouyang L; Ding H; Zhang T; Zhang K; Cheng S; Sun W Three-dimensional printing of Hela cells for cervical tumor model in vitro. Biofabrication 2014, 6, No. 035001. [PubMed: 24722236]

(54). Ventola CL Medical applications for 3D printing: current and projected uses. Pharm. Ther 2014, 39, 704.

(55). Colosi C; Shin SR; Manoharan V; Massa S; Costantini M; Barbetta A; Dokmeci MR; Dentini M; Khademhosseini A Microfluidic bioprinting of heterogeneous 3D tissue constructs using low-viscosity bioink. Adv. Mater 2016, 28, 677–684. [PubMed: 26606883]

(56). Zhang D; Shadrin IY; Lam J; Xian H-Q; Snodgrass HR; Bursac N Tissue-engineered cardiac patch for advanced functional maturation of human ESC-derived cardiomyocytes. Biomaterials 2013, 34, 5813–5820. [PubMed: 23642535]

(57). Zhu K; Shin SR; van Kempen T; Li Y-C; Ponraj V; Nasajpour A; Mandla S; Hu N; Liu X; Leijten J; Lin Y-D; Hussain MA; Zhang YS; Tamayol A; Khademhosseini A Gold nanocomposite bioink for printing 3D cardiac constructs. Adv. Funct. Mater 2017, 27, 1605352. [PubMed: 30319321]

(58). Izadifar M; Chapman D; Babyn P; Chen X; Kelly ME UV-assisted 3D bioprinting of nanoreinforced hybrid cardiac patch for myocardial tissue engineering. Tissue Eng., Part C 2018, 24, 74–88.

(59). Annabi N; Rana D; Sani ES; Portillo-Lara R; Gifford JL; Fares MM; Mithieux SM; Weiss AS Engineering a sprayable and elastic hydrogel adhesive with antimicrobial properties for wound healing. Biomaterials 2017, 139, 229–243. [PubMed: 28579065]

(60). Prasad R; Katiyar SK Crosstalk among UV-induced inflammatory mediators, DNA damage and epigenetic regulators facilitates suppression of the immune system. Photochem. Photobiol 2017, 93, 930–936. [PubMed: 27935057]

(61). Sato R; Harada R; Shigeta Y Theoretical analyses on a flipping mechanism of UV-induced DNA damage. Biophys. Physicobiol 2016, 13, 311–319. [PubMed: 28409083]

(62). Fedorovich NE; Oudshoorn MH; van Geemen D; Hennink WE; Alblas J; Dhert WJA The effect of photopolymerization on stem cells embedded in hydrogels. Biomaterials 2009, 30, 344–353. [PubMed: 18930540]

(63). Fessel G; Cadby J; Wunderli S; van Weeren R; Snedeker JG Dose- and time-dependent effects of genipin crosslinking on cell viability and tissue mechanics–Toward clinical application for tendon repair. Acta Biomater. 2014, 10, 1897–1906. [PubMed: 24384123]

(64). Oryan A; Kamali A; Moshiri A; Baharvand H; Daemi H Chemical crosslinking of biopolymeric scaffolds: Current knowledge and future directions of crosslinked engineered bone scaffolds. Int. J. Biol. Macromol 2018, 678.

(65). Jacot JG; McCulloch AD; Omens JH Substrate Stiffness Affects the Functional Maturation of Neonatal Rat Ventricular Myocytes. Biophys. J 2008, 95, 3479–3487. [PubMed: 18586852]

(66). Bansal S; Garg A; Khurana R; Chhabra P Platelet-rich fibrin or platelet-rich plasma–which one is better? an opinion. Indian J. Dent. Sci 2017, 9, 49.

(67). Wang H-L; Avila G Platelet rich plasma: myth or reality? Eur. J. Dent 2007, 1, 192. [PubMed: 19212466]

(68). Chang R; Emami K; Wu H; Sun W Biofabrication of a three-dimensional liver micro-organ as an in vitro drug metabolism model. Biofabrication 2010, 2, No. 045004. [PubMed: 21079286]

(69). Borie E; Oliví DG; Orsi IA; Garlet K; Weber B; Beltrán V; Fuentes R Platelet-rich fibrin application in dentistry: a literature review. Int. J. Clin. Exp. Med 2015, 8, 7922. [PubMed: 26221349]

(70). Bielecki T; Dohan Ehrenfest M, Platelet-rich plasma D (PRP) and Platelet-Rich Fibrin (PRF):surgical adjuvants, preparations for in situ regenerative medicine and tools for tissue engineering. Curr. Pharm. Biotechnol 2012, 13, 1121–1130. [PubMed: 21740380]

(71). Christman KL; Fok HH; Sievers RE; Fang Q; Lee RJ Fibrin glue alone and skeletal myoblasts in a fibrin scaffold preserve cardiac function after myocardial infarction. Tissue Eng. 2004, 10, 403–409. [PubMed: 15165457]

(72). Wendel JS; Ye L; Tao R; Zhang J; Zhang J; Kamp TJ; Tranquillo RT Functional effects of a tissue-engineered cardiac patch from human induced pluripotent stem cell-derived cardiomyocytes in a rat infarct model. Stem Cells Transl. Med 2015, 4, 1324–1332. [PubMed: 26371342]

(73). Liau B; Christoforou N; Leong KW; Bursac N Pluripotent stem cell-derived cardiac tissue patch with advanced structure and function. Biomaterials 2011, 32, 9180–9187. [PubMed: 21906802]

(74). Roura S; Soler-Botija C; Bagó JR; Llucià-Valldeperas A; Férnandez MA; Gálvez-Montón C; Prat-Vidal C; Perea-Gil I; Blanco J; Bayes-Genis A Postinfarction functional recovery driven by a three-dimensional engineered fibrin patch composed of human umbilical cord blood-derived mesenchymal stem cells. Stem Cells Transl. Med 2015, 4, 956–966. [PubMed: 26106218]

(75). Zhang G; Wang X; Wang Z; Zhang J; Suggs L A PEGylated fibrin patch for mesenchymal stem cell delivery. Tissue Eng. 2006, 12, 9–19. [PubMed: 16499438]

(76). Bellamy V; Vanneaux V; Bel A; Nemetalla H; Boitard SE; Farouz Y; Joanne P; Perier M-C; Robidel E; Mandet C; Hagège A; Bruneval P; Larghero J; Agbulut O; Menasché P Long-term functional benefits of human embryonic stem cell-derived cardiac progenitors embedded into a fibrin scaffold. J. Heart Lung Transplant 2015, 34, 1198–1207. [PubMed: 25534019]

(77). Son TI; Sakuragi M; Takahashi S; Obuse S; Kang J; Fujishiro M; Matsushita H; Gong J; Shimizu S; Tajima Y; Yoshida Y; Suzuki K; Yamamoto T; Nakamura M; Ito Y Visible light-induced crosslinkable gelatin. Acta Biomater. 2010, 6, 4005–4010. [PubMed: 20580950]

(78). Robinson M; Douglas S; Willerth SM Mechanically stable fibrin scaffolds promote viability and induce neurite outgrowth in neural aggregates derived from human induced pluripotent stem cells. Sci. Rep 2017, 7, 6250. [PubMed: 28740258]

(79). Di Y; Dye JF Fibrin crosslink stabilisation by glutaraldehyde for scaffold manufacture. In Tissue Engineering; Mary Ann Liebert Inc: 2007; pp 1696–1696.

(80). Maeda K; Alarcon EI; Suuronen EJ; Ruel M Optimizing the host substrate environment for cardiac angiogenesis, arterio-genesis, and myogenesis. Expert Opin. Biol. Ther 2017, 17, 435–447. [PubMed: 28274146]

(81). Chrobak MO; Hansen KJ; Gershlak JR; Vratsanos M; Kanellias M; Gaudette GR; Pins GD Design of a fibrin microthread-based composite layer for use in a cardiac patch. ACS Biomater. Sci. Eng 2017, 3, 1394–1403.

(82). Banks J; Board R; Carter J; Dodge A The cytotoxic and photodynamic inactivation of micro-organisms by Rose Bengal. J. Appl. Bacteriol 1985, 58, 391–400. [PubMed: 3997691]

(83). Maynard SJ; Menown IBA; Adgey AAJ Troponin T or troponin I as cardiac markers in ischaemic heart disease. Heart 2000, 371. [PubMed: 10722528]

(84). Oh H; Bradfute SB; Gallardo TD; Nakamura T; Gaussin V; Mishina Y; Pocius J; Michael LH; Behringer RR; Garry DJ; Entman ML; Schneider MD Cardiac progenitor cells from adult myocardium: homing, differentiation, and fusion after infarction. Proc. Natl. Acad. Sci. U. S. A 2003, 100, 12313–12318. [PubMed: 14530411]

(85). Huang J; Lu MM; Cheng L; Yuan L-J; Zhu X; Stout AL; Chen M; Li J; Parmacek MS Myocardin is required for cardiomyocyte survival and maintenance of heart function. Proc. Natl. Acad. Sci. U. S. A 2009, 106, 18734–18739. [PubMed: 19850880]

(86). Xiong Q; Hill KL; Li Q; Suntharalingam P; Mansoor A; Wang X; Jameel MN; Zhang P; Swingen C; Kaufman DS; Zhang J A fibrin patch-based enhanced delivery of human embryonic stem cell-derived vascular cell transplantation in a porcine model of postinfarction left ventricular remodeling. Stem Cells 2011, 29, 367–375. [PubMed: 21732493]

(87). Camelliti P; Green CR; Kohl P Structural and functional coupling of cardiac myocytes and fibroblasts In Cardiovascular Gap Junctions; Karger Publishers: 2006; Vol. 42, pp 132–149, DOI: 10.1159/000092566.

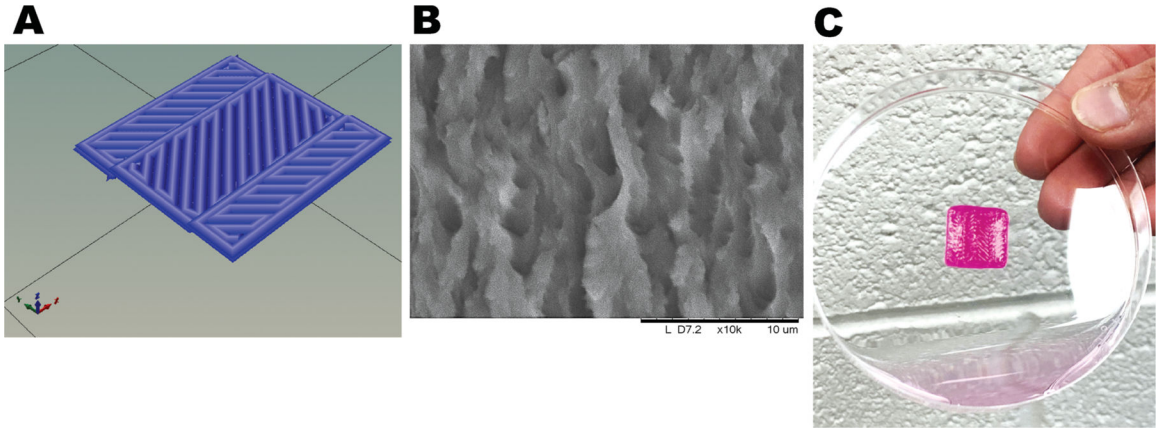

Figure 1.

Gross morphology of the structure printed using a fibrin–gelatin gel. (A) .stl file image. (B) Representative SEM en face image of a characteristic 3D printed pattern. (C) Herringbone construct casted with the bioprinter.

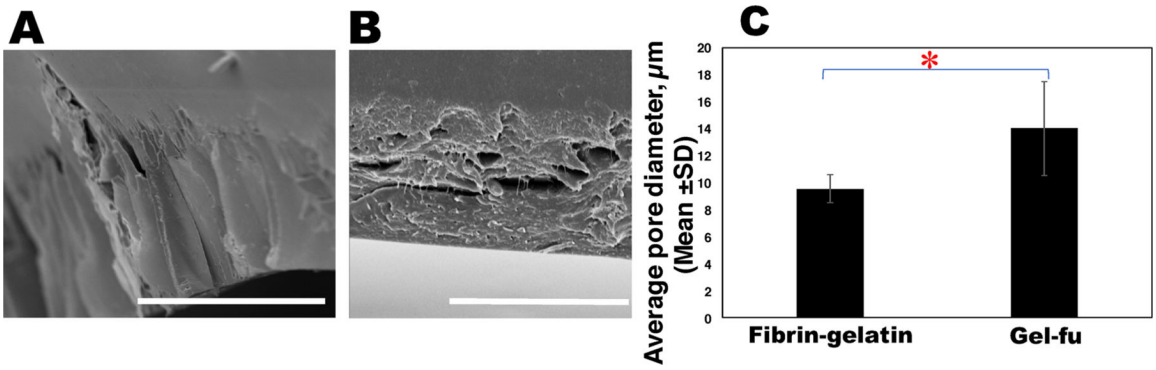

Figure 2.

SEM analysis for pore size estimation. (A) Representative SEM image of the edge of a characteristic fibrin–gelatin film. At least five representative images were acquired per sample and used to determine the average pore size depicted in (C), in comparison with the gel-fu (f-gelatin) structures as depicted in (B). (C) Plot comparing the average pore diameters for the fibrin–gelatin (current study)- and f-gelatin (gel-fu; previous study[12])-based constructs. The average pore diameters of the fibrin–gelatin films were significantly reduced (*$P < 0.05$) in comparison with gel-fu patterns from our previous study.[12] In (A), the scale bar corresponds to 50 μm, and in (B), it corresponds to 20 μm.

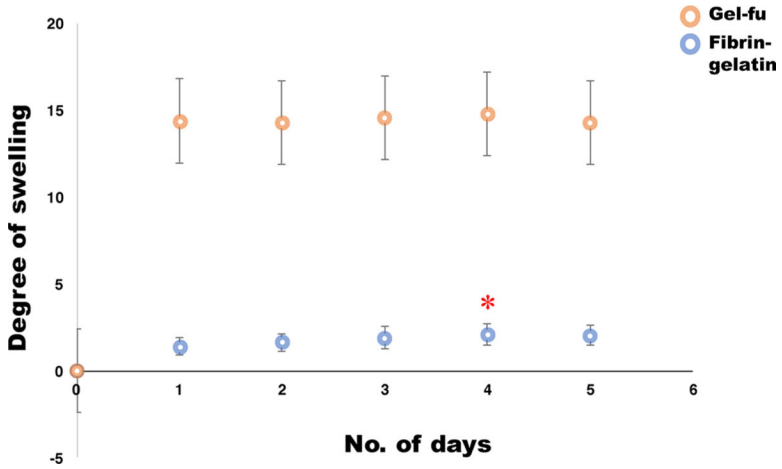

Figure 3.

Swelling analysis. Degree of swelling (mean ± SD) for a characteristic fibrin–gelatin-based pattern (blue circles) for over a period of 5 days for which the maximum degree of swelling was attained at day 4, significantly greater (*$P < 0.05$) than what was seen at previous time points. Beyond day 4, until day 5, the degree of swelling apparently reached equilibrium as these values did not seem to bear any statistical differences when analyzed. For comparison, a characteristic swelling degradation curve from a construct made with gel-fu (orange circles), as reported in our previous study,[12] is also included as controls.

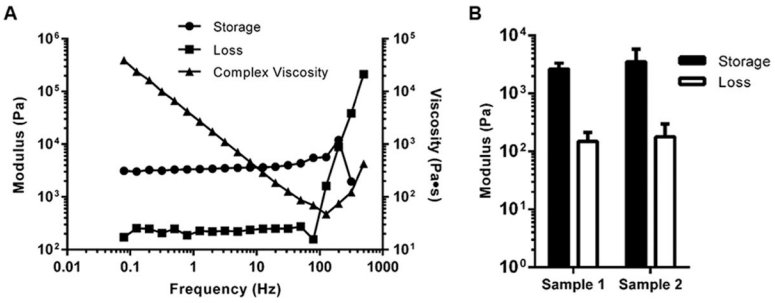

Figure 4.

Rheology analysis of fibrin–gelatin-based square structures. (A) Representative storage and loss moduli and complex viscosity from one characteristic gel sample. Therefore, it does not have error bars. (B) Average storage and loss moduli for similar sample patterns (#1 and #2, $n = 2$) analyzed during rheological characterization.

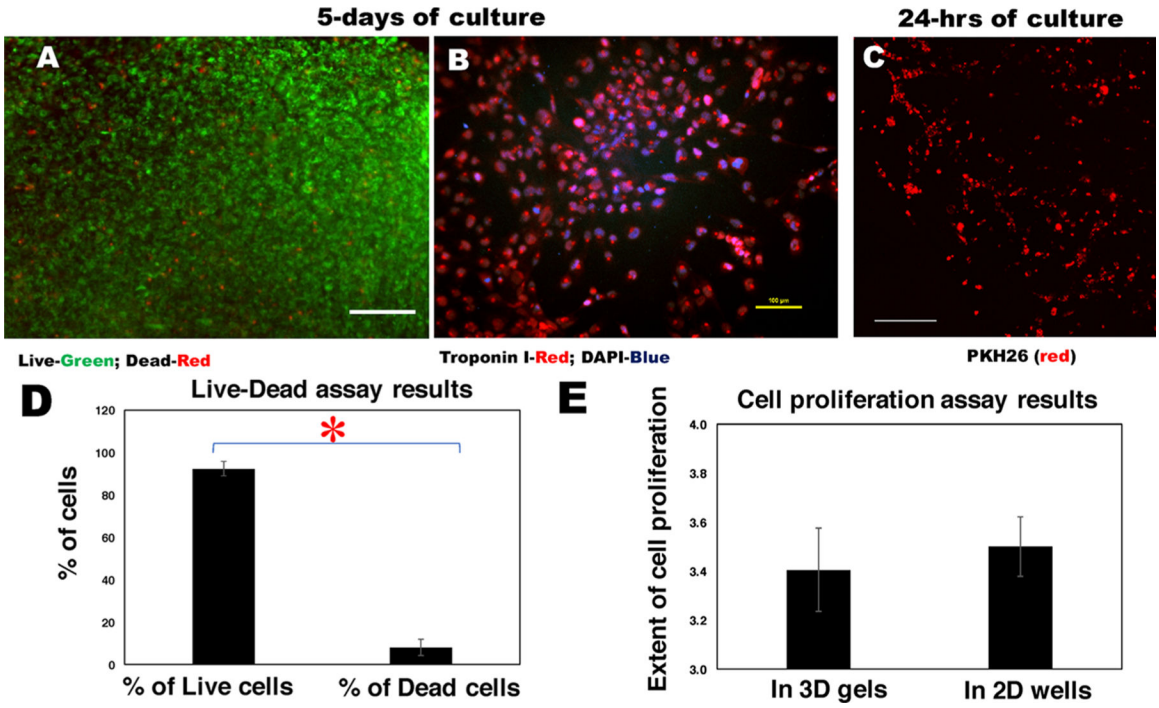

Figure 5.

Cell retention, viability, and proliferation. Characteristic images of human CM cell lines that were bioprinted within fibrin–gelatin patterns and (A) imaged using Live (green)/Dead (red) assay and (B) stained with troponin I antibody (red) and DAPI (blue) after 5 days of culture. In (A), the scale bar depicts 200 μm, and in (B), it is 100 μm. (C) PKH26 (red)-prestained cells bioprinted using a herringbone design were seen to align along this pattern after 24 h of culture in a maximum intensity projection of a *Z*-stack of confocal microscope images. Scale bar depicts 250 μm. (D) Quantification of cell viability estimated by Live/Dead assay and (E) the extent of live cell proliferation in samples. Statistically significant differences are denoted by an asterisk ($*P < 0.05$).

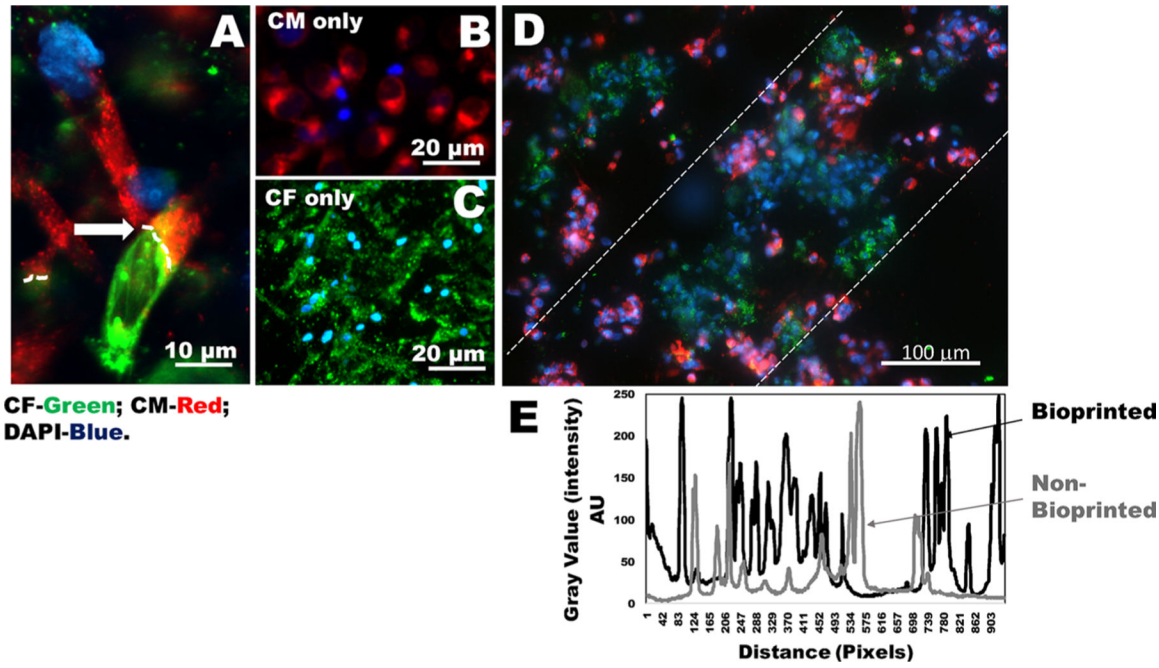

Figure 6.

Heterocellular coupling of CM and CF. (A) Human CM (prestained using PKH26, red) and CF (prestained using PKH67, green) coupled in 2D wells in the ratio of CM/CF (1:1) shown by white arrows and dotted lines. (B, C) Images of controls for either CM or CF (in 2D wells). (D) Results of heterocellular coupling between prestained CM (red) and CF (green) from 3D bioprinted constructs. Nonprinted controls that included cells mixed in gels are shown in Figure S5. The white dashed lines in (D) denote that the cells are confined to their printed patterns. However, these samples were fixed prior to DAPI staining, and the cells were not viable during imaging. To confirm heterocellular coupling using viable cells, we report results in Figure 7. (E) Intensity values within the white dotted lines in a bioprinted sample (black line) versus a nonbioprinted sample (gray line). The average intensity values for the bioprinted samples exhibited more frequent peaks with respect to distance, depicting a higher frequency of cells present in the preferred orientation compared to samples that were nonbioprinted.

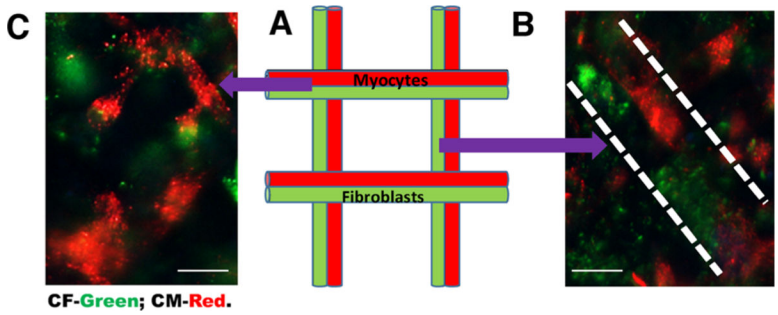

Figure 7.

Heterocellular coupling of nonfixed CM and CF in 3D bioprinted gels. Viable and nonfixed cells used to confirm heterocellular coupling between CM and CF. (A) Schematic of a lattice grid pattern for coculturing of CM (red) and CF (green). (B) Human CM (red) and CF (green) coupled when confined to two adjacent line patterns (as denoted by white dashed lines). (C) Representative cell coupling in junctions of the grid pattern. Although cell coupling may be occurring in cells mixed and cross-linked within gels, it is very difficult to confirm in samples, which are not patterned distinctively using bioprinting, as shown in Figure S5. Scale bars depict 10 μm.

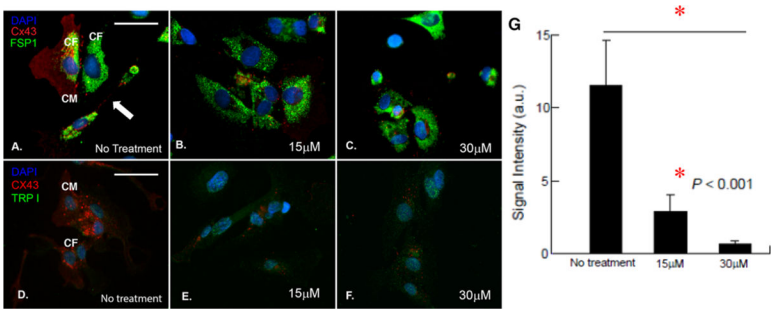

Figure 8.

Confirmation of heterocellular coupling between CM and CF. (A–C) Cocultured cells immunostained with Cx43 (red), FSP-1 (green), and DAPI (blue) with no Gap26 treatment (A) and with 15 μM (B) and 30 μM Gap26 (C). (D–F) Cocultured cells immunostained with Cx43 (red), troponin I (TRP I, green), and DAPI (blue) with no Gap26 treatment (D) and with 15 μM (E) and 30 μM Gap26 (F). Scale bars in (A)–(F) are of the same size and correspond to 50 μM. (G) Average signal intensity of Cx43 expression in cultures with no Gap26 treatment and with 15 μM (B) and 30 μM Gap26.

Table 1.

Optimization of the Fibrinogen Solution and Amounts of Furfuryl–Gelatin for Making of Bioink

solution no.	fibrinogen	gel-fu	Rose Bengal (RB)	state of the bioink	observations post printing
1	1 mL of 60 mg/mL	150 mg	50 mg (5% w/v as per our previous study[12])	highly viscous with clumps, in addition black lumps were noted	the printed structure was incomplete and discontinuous, but the sample did not degrade for 4 days
2	1 mL of 60 mg/mL	100 mg	50 mg	less viscous than #1, but clumps were present	the printed structure was incomplete and discontinuous, but the sample did not degrade for 4 days
3	990 μL of 60 mg/mL (~59.4 mg/mL)	155 mg	10 μL solution aliquot from a stock of 5% (w/v)	the solution appeared to have sufficient viscosity to enable printing	printed a clear rectangular sheet easily and structural fidelity was maintained for 4 days
4 (control)	1 mL of 60 mg/mL	150 mg of porcine gelatin	none used	looked ideal for printing; not too thick or watery	printed a neat two-layered sheet; however, the structure dissolved much earlier than the above samples